4D Electrical Resistivity Imaging of Stress Perturbations Induced During High-Pressure Shear Stimulation Tests

T. C. Johnson[1], J. Burghardt[1], C. Strickland[1], D. Sirota[1], V. Vermeul[1], H. Knox[1], P. Schwering[2], D. Blankenship[2] and T. Kneafsey[3] and the EGS Collab Team

[1]Pacific Northwest National Laboratory, Richland Washington, USA

[2]Sandia National Laboratories, Albuquerque New Mexico, USA

[3]Lawrence Berkeley National Laboratory, Berkeley California, USA

Corresponding author: Tim Johnson (tj@pnnl.gov)

Key Points:

- Remotely monitoring stress is challenging but important for relating geomechanical behavior to flow pathways during energy production
- Bulk electrical conductivity is sensitive to stress in crystalline rock
- Time-lapse electrical resistivity tomography can be used to remotely monitor 3D changes in effective stress

Abstract

Fluid flow through fractured media is typically governed by the distribution of fracture apertures, which are in turn governed by stress. Consequently, understanding subsurface stress is critical for understanding and predicting subsurface fluid flow. Although laboratory-scale studies have established a sensitive relationship between effective stress and bulk electrical conductivity in crystalline rock, that relationship has not been extensively leveraged to monitor stress evolution at the field scale using electrical or electromagnetic geophysical monitoring approaches. In this paper we demonstrate the use time-lapse 3-dimensional (4D) electrical resistivity tomography to image perturbations in the stress field generated by pressurized borehole packers deployed during shear-stimulation attempts in a 1.25 km deep metamorphic crystalline rock formation.

Plain Language Summary

Time-lapse electrical geophysical sensing is used to image 3D changes in rock stress generated by an isolated and pressurized interval of a borehole in a deep, dense, fractured rock formation.

1 Introduction

Enhanced Geothermal Systems (EGS) offer a tremendous potential source of clean baseload energy to support the energy security of the United States (Augustine, 2016). EGS involves the

challenging task of establishing hydraulic connections between two or more boreholes in deep, hot, dry rock, whereby fluid may be circulated to extract thermal energy. Successful EGS development requires improved understanding and control of EGS reservoir stimulation, where fractures are generated and/or enhanced to provide effective heat-exchanging flow pathways between injection and production wells. Stimulation processes and long-term efficacy are governed in large part by both the natural state of stress and the evolution of stress during stimulation and operation (Min, Rutqvist, Tsang, & Jing, 2004; Zoback & Byerlee, 1975a, 1975b). Consequently, developing improved methods of understanding and monitoring stress are important for EGS development (Pyrak-Nolte, 2015).

The EGS-Collab project was funded by the U.S. Department of Energy, Geothermal Technologies Office, to conduct fracture stimulation studies in a highly instrumented field research testbed at EGS-relevant stress states (T. Kneafsey, 2022). Experiment #1, which focused on executing and monitoring hydrofracture stimulations, was conducted on the 4850 Level of the Sanford Underground Research Facility (SURF) in Lead, South Dakota, approximately 1.5 km below ground surface (bgs) (Fu et al., 2021; Heise, 2015). In Experiment #2, shear stimulation testing was conducted on the 4100 Level of SURF, which lies approximately 1.25 km bgs (T. Kneafsey, 2022). Shear stimulation involves isolating and pressurizing an existing fracture below the minimum principle stress (to avoid hydrofracturing) in an attempt shear-slip the fracture and create a self-propped hydraulic connection between two boreholes. Shear stimulation was attempted at approximately 10 candidate locations, none of which resulted in a successful shear slip, or any fluid injected into the formation. In addition to extensive pressure, flowrate, and fluid conductivity monitoring, each attempt was closely monitored using 4D cross-borehole seismic, fiber-based distributed temperature and strain, and 4D electrical resistivity tomography (ERT).

In this paper, we demonstrate how 4D ERT monitoring was used to image stress-induced perturbations in bulk electrical conductivity (BEC) during Experiment #2 shear stimulation attempts at six different depths. During each stimulation attempt, a section of the borehole was isolated and pressurized using a pair of straddle packers. Compressive stresses exerted on the borehole wall by the packers and pressurized interval induced an effective stress perturbation 'bulb' around the interval, and a consequent decrease in porosity (and therefore BEC) within the stress bulb. The resulting decrease in BEC within the stress bulb was then imaged in 3D using ERT electrodes deployed within surrounding monitoring boreholes. Although the sensitivity of BEC to stress in crystalline rock is well documented at the laboratory scale (Brace, 1975; Brace & Orange, 1966; Brace, Orange, & Madden, 1965; Kaselow & Shapiro, 2004), field-scale efforts to infer stress evolution using electrical or electromagnetic geophysical methods are limited. Because there was no flow within the formation during the stimulation attempts, changes in BEC during stimulation are uniquely attributeable to changes in stress. Comparisons of ERT images collected between shear stimulation attempts and a follow-on hydrofracture simulation show that the 3D stress perturbation patterns generated during shear stimulation attempts provided insight regarding the hydrofracture location and orientation. In addition to demonstrating the field-scale sensitivity of BEC to stress at EGS-relevant depths and pressures, results also point to the possibility of new approaches for EGS monitoring and for inferring in-situ rock properties.

We begin by describing the Experiment #2 testbed and the shear stimulation sequences, which end with a hydrofracture stimulation. We then present the ERT imaging results and corresponding interpretation. Finally we conclude with a discussion of the results and possible

new avenues for inferring in-situ bulk modulus and intrinsic permeability using ERT monitoring of stress perturbations.

2 EGS-Collab Experiment #2 Testbed

Experiment #2 of the EGS-Collab project was conducted on the 4100 Level of SURF, which lies ~1.25 km (4100 ft) below the ground surface. Testing boreholes were installed within an amphibolite sequence known as the Yates member of the Poorman Formation, consisting of metamorphosed basalt to form a massive hornblende-plagioclase amphibolite schist, with lesser amounts of quartz and calcite(Caddey, 1991). Figure 1 shows the testbed layout, consisting of nine subhorizontal boreholes originating at the eastern wall of the drift. Four dedicated geophysical monitoring boreholes originating at sites A and C (AMU, AML, DMU and DML) were instrumented with seismic sources and receivers, multi-mode (temperature and strain) sensing fiber, and ERT electrodes, all grouted in place. The remaining five boreholes orginating from site A were left open to enable multiple-use configurations including geophysical instrumentation or zonal isolation packers for precisely-located pressure monitoring and flow control. For Experiment 2, boreholes Tn, Tu, Ts and Tl were instrumented with ERT electrodes, with Ts also including seismic sources and receivers. Borehole Tc was oriented to maximize the probability of shear slip during stimulation, given what was known about the in-situ stress field (Burghardt et al., 2022).

Shear stimulation attempts were conducted by isolating (using a straddle packer system) and pressurizing targeted sections of Tc where potential shearable fracture intervals were identified through core inspection. Here, we focus on shear stimulation intervals I1-I6 shown in Figure 1A. Each interval (green or black) shows the corresponding pressurized interval for each test, which includes the ~2 m pressurized interval bounded on each end by borehole packers. The inset photograph in Figure 1B was taken inside the 4100 Level drift during testbed construction just south of Site B facing northward to Site A.

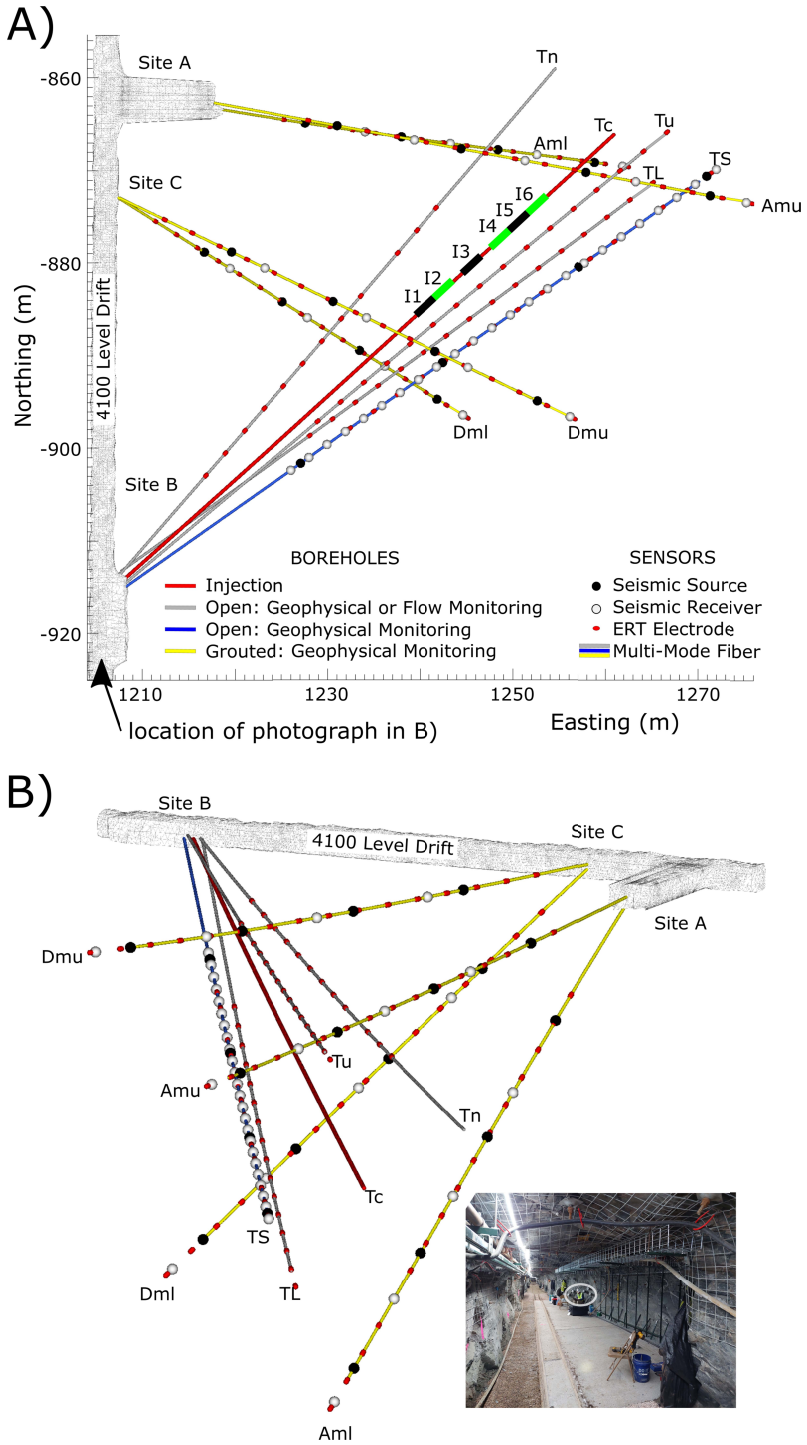

Figure 1. A) Plan and B) Oblique views of the experimental testbed including borehole orientations with ERT and seismic instrumentation locations. Intervals I1-I6 (black and green)in A) denote isolated sections of borehole Tc that were pressurized during shear stimulation attempts. The inset image in B) is a photograph taken during testbed construction, standing in the drift at -917 m northing and facing northward (as annotated in A). Kickoff points for Site B boreholes are located within the white outline.

3 Shear Stimulation Experiments

A primary objective of Experiment #2 was to shear-slip a natural fracture in borehole Tc and generate a self-propped hydraulic connection between Tc and one or more of the Site B boreholes. Each shear experiment proceeded by isolating a ~2 m interval of the borehole (Figure 1, I1-I6) using a pair of straddle packers, each packer being ~1.5 m long for a total length of 5 m. After the pressure of each packer was raised to 10.34 MPa (1500 psi), the interval flowrate was recorded as the interval pressure was raised to 16.25 MPa (2350 psi), which is approximately 83% of the previously estimated minimum principle stress (T. Kneafsey, 2022) and approximately 30% of the estimated interval pressure required to generate tensile stress at the interval wall. Interval pressure was then held at 16.25 MPa for at least 30 minutes while interval flowrate was recorded. In every case, zero interval flow was recorded during the hold period, indicating an unsuccessful shear stimulation attempt. Figure 2 shows a typical flowrate and interval pressure timeseries during a shear stimulation attempt, Tc interval I1 (Figure 1A) in this case.

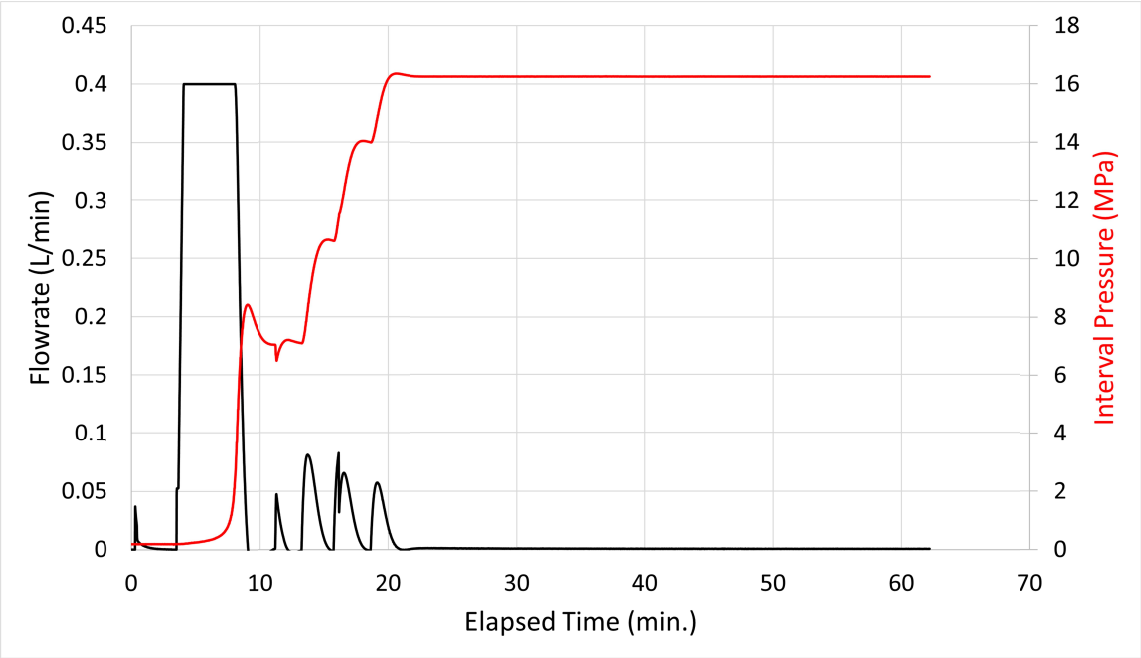

Figure 2. Flowrate and interval pressure for shear stimulation attempt in wellbore Tc interval I1 (Figure 1A). Flowrate variations during the first ~20 minutes occur during interval pressure-up (i.e. there is no flow into the formation).

4 ERT Monitoring During Stimulation Attempts

ERT data were collected in a pole-pole like configuration. A single measurement was collected by injecting current between one of the electrodes shown in Figure 1 and a remote electrode. During the current injection, the induced potential was measured between one or more of the electrodes shown in Figure 1 and a second remote electrode, which provided the potential reference for all measurements. As shown by the inset photograph in Figure 1B, continuous metallic wire mesh was installed on the ceiling and walls of the drift for rockfall protection, pinned to the rock using metallic rock bolts on a ~2m grid. Electrical coupling between the mesh, rock bolts, and rock effectively formed a zero-potential reference surface on the ceiling and walls

of the drift. With this in mind, we used the mesh as both the current sink and potential reference electrode for all measurements.

Measurements were collected using an 8-channel ERT data acquisition system, meaning eight potential measurements were collected for each current injection. Pre-stimulation baseline surveys were collected continuously for two days and analyzed to remove data with small signal to noise ratios, which were generally associated with measurements where the potential electrode was far from the current electrode. For the 124 electrodes in the array, the full pole-pole survey consisted of 7749 measurements. After filtering, 3615 of those measurements were deemed outside of the noise envelope and were collected during the time-lapse imaging phase. The time interval between ERT survey times, or equivalently between ERT images, was approximately 46 minutes.

5 ERT Data Processing

Surveys were collected continuously during the shear stimulation attempts. After each survey, data were autonomously transferred to offsite computing resources and processed. Data were inverted in parallel on 66 processing cores using the open source E4D software (https://e4d.pnnl.gov). The total time between the beginning of a survey and delivery of the resulting ERT image was approximately 55 minutes. Drift boundaries were located using LiDAR sensing, which enabled the drift boundaries to be precisely simulated using an unstructured tetrahedral mesh. Elements inside of the drift boundaries were removed to simulate zero current flux conditions across drift boundaries. Constant potential conditions along the drift walls and ceilings caused by the rockfall protection mesh were simulated using the metallic infrastructure modelling method described by (Johnson & Wellman, 2015).

Baseline BEC structure was established by inverting one of the ERT data sets collected prior to the stimulation attempts. Occam's-type regularization constraints were imposed by enforcing nearest-neighbor smoothing, whereby the difference in BEC between neighboring elements was minimized, subject to fitting the data. Two different constraints were imposed to regularize the time lapse inversions of data collected during shear stimulation events. First, the change in BEC from the previous time-step between neighboring cells was minimized, which enforces smoothness in the change in BEC in both space and time. Second, changes in BEC were constrained to be negative with respect to baseline BEC conditions. The second constraint is justified based on the assumption that unless fluid was injected into the formation, there was no active mechanism to increase BEC during the time-lapse imaging. That is, we assumed no increase in porosity, fluid conductivity, or temperature within the formation during the shear stimulation attempts. To the contrary, the increased compressive stress with respect to baseline imposed by the pressurized stimulation interval decreased porosity, leading to a corresponding decrease in BEC (Brace & Orange, 1966; Brace et al., 1965). Had fluid been introduced into the formation during the shear stimulation attempts, the inversion would have been re-run without the negativity constraint, as was done with the time-lapse inversion of the hydrofracture stimulation.

6 ERT Imaging Results

178 ERT imaging results for each of the six stimulation intervals are shown in Figures 3 and 4.
179 Changes in BEC from baseline are shown as iso-surfaces in plan and oblique views for each
180 stimulation event. In each case, changes in BEC are negative with respect to baseline conditions
181 and focus around the pressurized injection interval. Decreases in BEC mirror the anticipated
182 effective stress perturbation, in that the largest magnitudes occur at, and decay with distance
183 from, the pressurized interval. The relationship between stress and BEC can be described as
184 follows (Brace, 1975; Johnson et al., 2021; Kaselow & Shapiro, 2004):

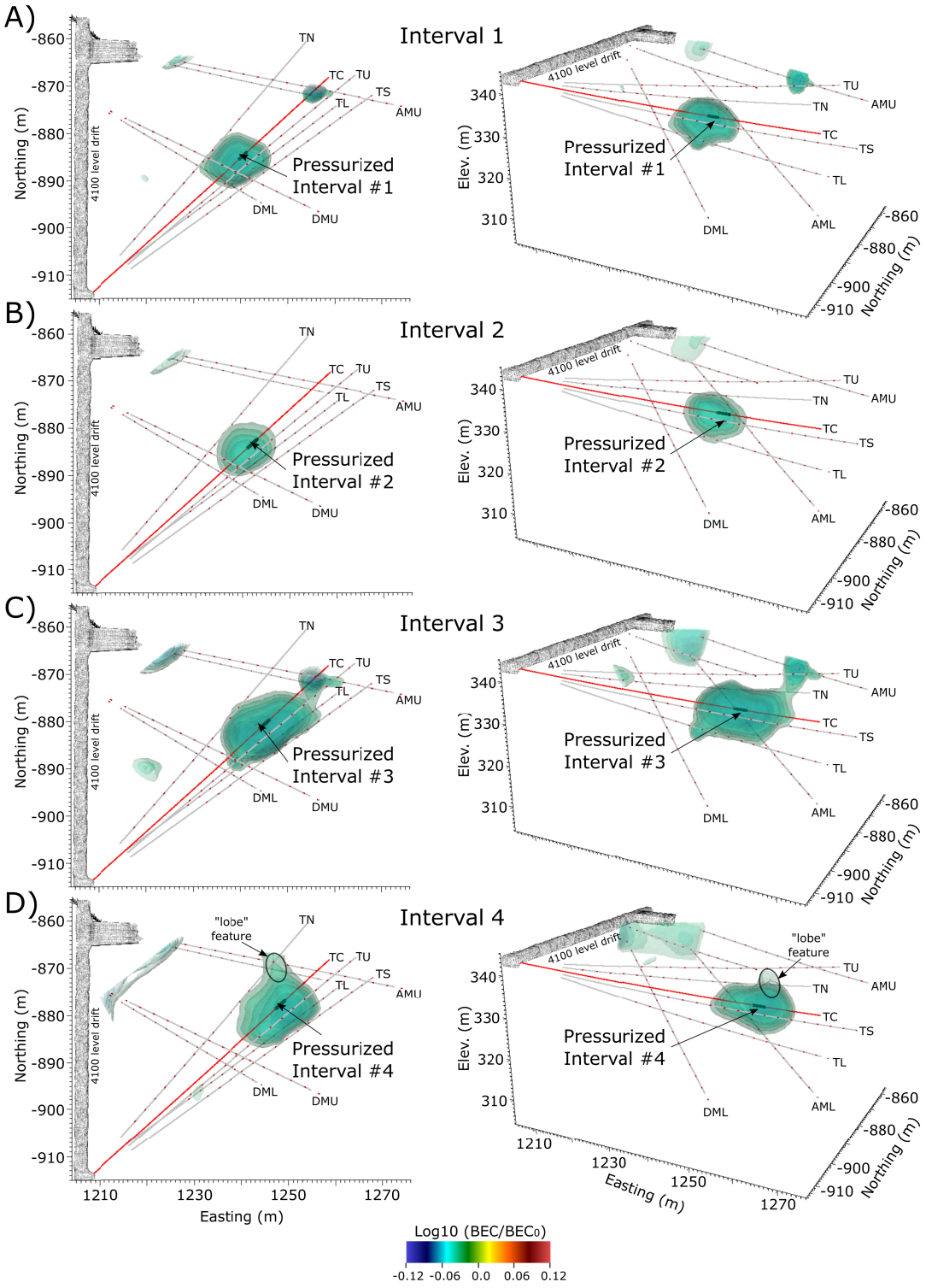

Figure 3. ERT-derived changes in BEC during shear stimulation attempts in intervals 1-4. Decreases in BEC are caused by stress-induced decreases in porosity around the pressurized interval.

When the interval is pressurized, the surrounding host rock experiences a corresponding increase in total stress. In response, compliant microfractures compress, resulting in a decrease in porosity, and a corresponding decrease in BEC. The stress-induced decrease in porosity requires

that either the pore water compresses within the pore space, or the pore water migrates out of the pore space. Although meausurements of host rock compressibility (or its inverse, bulk modulus) aren't available, we assume that, like other dense crystalline rocks, rock compressibility is less than that of water at the same temperature and pressure. For example, the compressibility of water at standard temperature and pressure is approximately 5E-10 GPa^{-1} (Schmitt, 2015). In contrast, Davarpanah et al. (2020) reported the compressibility of unaltered granite and horneblende schist at approximately 2.9E-10 GPa^{-1} and 1.3E-10 GPa^{-1} respectively . If these compressibilities approximate testbed conditions, then it is reasonable to assume that the decrease in porosity occurred coincident with pore water compression, as opposed to pore water migration. The same assumption is supported by the lack of flow from the pressurized interval (Figure 2).

Figure 4C shows the change in BEC from a survey collected during the hydrofracture stimulation and flow test in interval 4, after initiation of the hydrofracture. The fracture breakthrough point on wellbore AMU was recorded as a strain purterbation on distributed strain sensing (DSS) fiber at the location shown (Kneafsey et al., 2023). Like the shear stimulation attempt in interval 4 (Figure 3D), a negative BEC anomaly develops around the pressurized interval. However, in this case, the anomaly is more elongated along the projection of the hydrofracture from interval 4 to AMU, and is presumably caused by the compressive stress exerted normal to the pressurized hydrofracture. Although the hydrofracture itself represents an increase in BEC from baseline, the ERT response is negative, and therefore dominated by the by the stress exerted on the host rock by the pressurized hydrofracture in this case.

Figure 4C also shows a BEC anomaly centered around borehole AMU that transitions from a positive BEC anomaly to a negative BEC at the point of the hydrofracture intersection. The shallower positive anomaly is caused by high-pressure fluid migrating from the hydrofracture into AMU and toward the drift. Although AMU was grouted, flow (dripping ~10 ml/min) from AMU was observed shortly after stimulation, confirming that pressurized water was entering the borehole. The deeper negative anomaly surrounding AMU is presumably caused by compressive forces exerted normal to the pressurized hydrofracture on AMU, which is likely more compliant than the host rock. The consequent compression of AMU near the hydrofracture results in a decrease in porosity, and a subsequent decrease in BEC at the borehole.

The positive BEC anomaly that develops around borehole TN is also caused by fluid inflow, confirmed by outflow from the wellhead in the drift. In contrast to borehole AMU, borehole TN was not grouted and open to atmospheric pressure. Inflow into TN suggests the hydrofracture intersected TN. However, unlike AMU, the point at which the hydrofracture intersects TN is not indicated by the BEC anomaly. The deepest point of the BEC anomaly surrounding TN occurs at the last electrode in TN (Figure 1A), which is the deepest point of sensitivity to fluid influx. The hydrofracture intersection with TN likely occurs deeper in the borehole.

7 Discussion

The footprint of the BEC anomaly appears to vary considerably between shear stimulation attempts (Figure 3A-3D, Figure 4A-4B). Although this may be an artifact of variable spatial resolution caused by the non-uniform distribution of electrodes, it is the opinion of authors that

differences in the size of the BEC anomalies are caused by temporal 'smearing'. In intervals 1, 2 and 6, the time taken for a stimulation attempt was slightly less than the time required to complete a full ERT survey. Consequently, some fraction of ERT data were collected when the interval was not pressurized, which would naturally result in a smaller BEC anomaly.

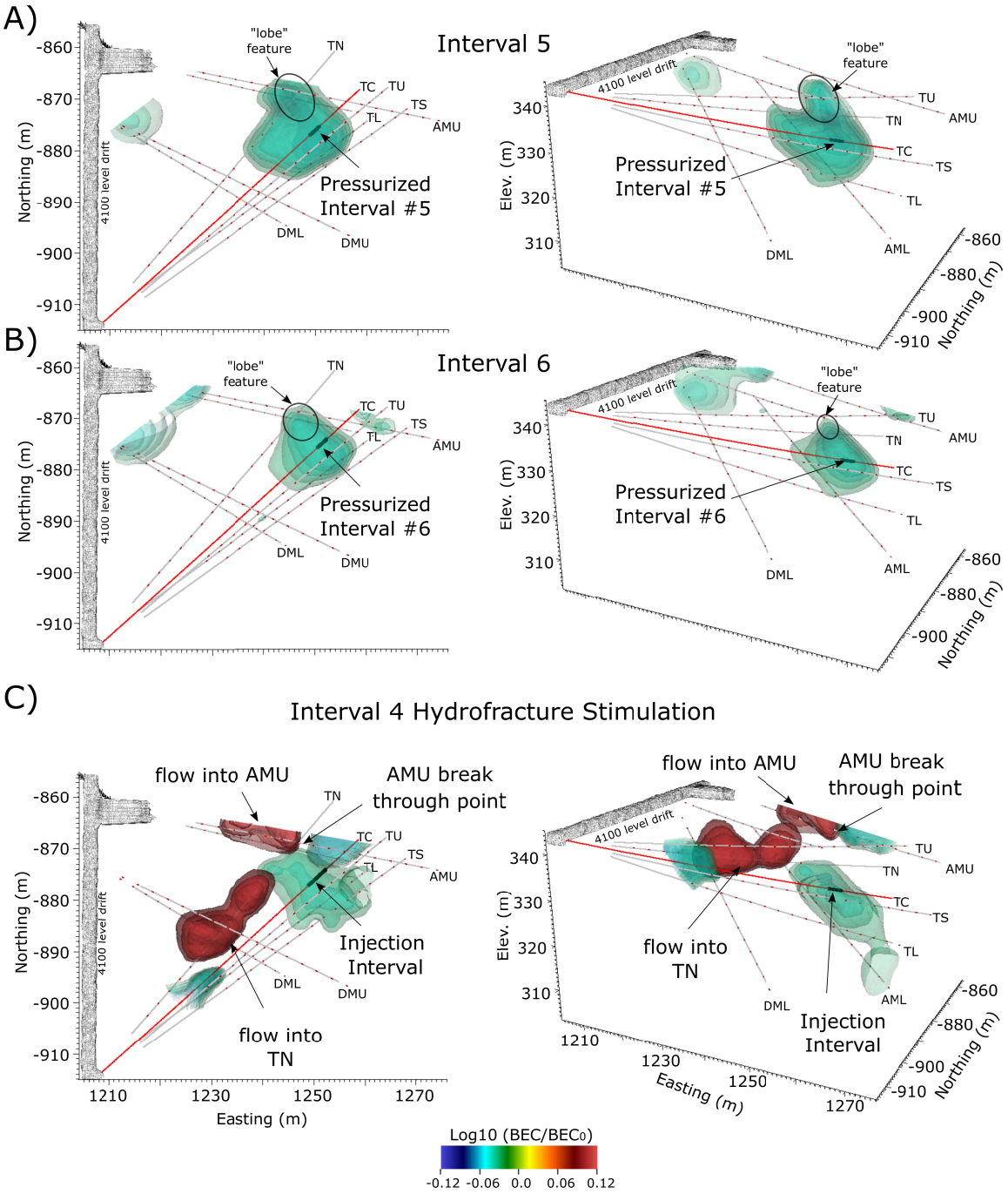

Figure 4. ERT-derived changes in BEC during shear stimulation attempts in intervals 5 and 6 (4A and 4B) and during the hydrofracture stimulation (4C) . Decreases in BEC are caused by stress-induced decreases in porosity around the pressurized interval. The annoted 'lobe' feature observed during shear stimulation attempts 4-6 (Figures 3D, 4A and 4B) is co-located with the projection of the hydrofracture from the injection interval to the break through point on wellbore AMU.

The relative shape of the BEC anomaly also varies considerably between shear stimulation attempts. Intervals 1 and 2 display a relatively uniform ovoid shape around the pressurized zone with the long axis parallel to the borehole. In contrast, intervals 3-6 develop a lobe that extends northward and vertically toward the TN and AMU boreholes. Noteably, the lobe extending from interval 4 follows the same trajectory as the hydraulic fracture stimulated from interval 4 (Figures 3D and 4C). This suggests that the BEC lobe was located in a zone of relatively compliant rock that ultimately fractured during the interval 4 hydrostimulation. Upward and northward trending BEC lobes extending from intervals 5 and 6 (Figure 4, upper two panels) appear to be caused by the same region of comparatively decreased bulk modulus.

In addition to providing information regarding stress perturbations during the stimulation attempts, time-lapse ERT may lead to new approaches for the in-situ measurement of intrinsic permeability under low permeability conditions like those found in the Experiment #2 testbed. For instance, consider the case where a borehole is instantaneously 'dry-pressurized' by a single packer to impose zero-flow increase in stress on the borehole wall. As described above, the resulting increase in total stress adjacent to the packer causes a decrease in BEC. Compression of the pore space adjacant to the packer will induce a pore pressure gradient, causing pore water to migrate down gradient at a rate that is dependent on permeability. As pore water migrates down gradient, pore pressure decreases, thereby increasing the effective stress on the rock matrix, increasing compression of compliant pore spaces, and decreasing the BEC. If ERT measurements were collected fast enough to sense the time-evolution of the BEC anomaly, those measurements could conceptually be used to estimate in-situ intrinsic permeability of host rock near the pressurized interval.

8 Conclusions

At the field scale, we have demonstrated the sensitivity of BEC to changes in stress in saturated crystalline rocks that have been widely observed in laboratory scale settings. The relationship between increases in stress and decreases in BEC enabled time-lapse ERT to image, in 3D, the effective stress perturbation that developed around a set of pressurized borehole packers. Imaging results provided information regarding the location and orientation of a relatively compliant region of rock that ultimately fractured during hydrostimulation and provided the primary flow pathway. These results speak to the possibility of enabling enhanced understanding and control by using electrical and electromagnetic geophysical sensing methods to remotely monitor stress and flow-path evolution in deep subsurface reservoirs (i.e. enhanced geothermal, carbon sequestration, and oil and gas).

Acknowledgments

This material was based upon work supported bythe U.S. Department of Energy, Office of Energy Efficiency and Renewable Energy (EERE), Office of Technology Development, Geothermal Technologies Office, under Award Number DE-AC05-76RL01830. The United States Government retains, and the publisher, by accepting the article for publication, acknowledges that the United States Government retains a non-exclusive, paid-up, irrevocable, world-wide license to publish or reproduce the published form of this manuscript, or allow others to do so, for United States Government purposes.

Sandia National Laboratories is a multimission laboratory managed and operated by National Technology & Engineering Solutions of Sandia, LLC, a wholly owned subsidiary of Honeywell International Inc., for the U.S. Department of Energy's National Nuclear Security Administration under contract DE-NA0003525.

This paper describes objective technical results and analysis. Any subjective views or opinions that might be expressed in the paper do not necessarily represent the views of the U.S. Department of Energy or the United States Government. The research supporting this work took place at the Sanford Underground Research Facility in Lead, South Dakota. The assistance of the Sanford Underground Research Facility and its personnel in providing physical access and general logistical and technical support is gratefully acknowledged.

Open Research

ERT monitoring data, meta data, and E4D ERT data processing files may be accessed through the U.S. Department of Energy Geothermal Data Repository at https://gdr.openei.org/submissions/1480. E4D source code and documentation is available at https://e4d.pnnl.gov. Flow and pressure data collected during testing may be accessed through the Geothermal Data Repository at https://dx.doi.org/10.15121/1988394.

Figures

Figure 1. A) Plan and B) Oblique views of the experimental testbed including borehole orientations with ERT and seismic instrumentation locations. Intervals I1-I6 (black and green)in A) denote isolated sections of borehole TC that were pressurized during shear stimulation attempts. The inset image in B) is a photograph takend during testbed construction, standing in the drift at -917 m northing and facing northward. Kickoff points for Site B boreholes are located within the white outline.

Figure 2. Flowrate and interval pressure for shear stimulation attempt in wellbore Tc interval I1 (Figure 1A). Flowrate variations during the first ~20 minutes occur during interval pressure-up (i.e. there is no flow into the formation).

Figure 3. ERT-derived changes in BEC during shear stimulation attempts in intervals 1-4. Decreases in BEC are caused by stress-induced decreases in porosity around the pressurized interval.

Figure 4. ERT-derived changes in BEC during shear stimulation attempts in intervals 5 and 6 (4A and 4B) and during the hydrofracture stimulation (4C) . Decreases in BEC are caused by stress-induced decreases in porosity around the pressurized interval. The annoted 'lobe' feature observed during shear stimulation attempts 4-6 (Figures 3D, 4A and 4B) is co-located with the projection of the hydrofracture from the injection interval to the break through point on wellbore AMU.

References

Augustine, C. (2016). Update to Enhanced Geothermal System Resource Potential Estimate, *GRC Transactions, 40*(6).

Brace, W. F. (1975). Dilatancy-Related Electrical-Resistivity Changes in Rocks. *Pure and Applied Geophysics, 113*(1-2), 207-217. doi:Doi 10.1007/Bf01592911

Brace, W. F., & Orange, A. S. (1966). Electrical Resistivity Changes in Saturated Rock under Stress. *Science, 153*(3743), 1525-&. doi:DOI 10.1126/science.153.3743.1525

Brace, W. F., Orange, A. S., & Madden, T. R. (1965). Effect of Pressure on Electrical Resistivity of Water-Saturated Crystalline Rocks. *Journal of Geophysical Research, 70*(22), 5669-+. doi:DOI 10.1029/JZ070i022p05669

Burghardt, J., Knox, H. A., Doe, T., Blankenship, D., Schwering, P., Ingraham, M., . . . Roggenthen, W. (2022). *EGS Stimulation Design with Uncertainty Quantification at the EGS Collab Site.* Paper presented at the American Rock Mechanics Association U.S. Rock Mechanics/Geomechanics Symposium, Santa Fe, New Mexico.

Caddey, S. W., Bachman, R. L., Campbell, T. J., Reid, R.R., Otto, R. P. . (1991). *The Homestake gold mine, an early Proterozoic iron-formation-hosted gold deposit, Lawrence County, South Dakota*. Retrieved from https://doi.org/10.3133/b1857J

Davarpanah, S. M., Ván, P., & Vásárhelyi, B. (2020). Investigation of the relationship between dynamic and static deformation moduli of rocks. *Geomechanics and Geophysics for Geo-Energy and Geo-Resources, 6*(1). doi:ARTN 29

10.1007/s40948-020-00155-z

Fu, P. C., Schoenball, M., Ajo-Franklin, J. B., Chai, C. P., Maceira, M., Morris, J. P., . . . Team, E. C. (2021). Close Observation of Hydraulic Fracturing at EGS Collab Experiment 1: Fracture Trajectory, Microseismic Interpretations, and the Role of Natural Fractures. *Journal of Geophysical Research-Solid Earth, 126*(7). doi:ARTN e2020JB020840

10.1029/2020JB020840

Heise, J. (2015). The Sanford Underground Research Facility at Homestake. *Proceedings of the South Dakota Academy of Science, Vol 94, 94*, 347-347.

Johnson, T. C., Burghardt, J., Strickland, C., Knox, H., Vermeul, V., White, M., . . . Team, E. C. (2021). 4D Proxy Imaging of Fracture Dilation and Stress Shadowing Using Electrical Resistivity Tomography During High Pressure Injections Into a Dense Rock Formation. *Journal of Geophysical Research-Solid Earth, 126*(11). doi:ARTN e2021JB022298

10.1029/2021JB022298

Johnson, T. C., & Wellman, D. (2015). Accurate modelling and inversion of electrical resistivity data in the presence of metallic infrastructure with known location and dimension. *Geophysical Journal International, 202*(2), 1096-1108. doi:10.1093/gji/ggv206

Kaselow, A., & Shapiro, S. A. (2004). Stress sensitivity of elastic moduli and electrical resistivity in porous rocks. *Journal of Geophysics and Engineering, 1*(1), 1-11. doi:Pii S1742-2132(04)73747-4

10.1088/1742-2132/1/1/001

Kneafsey, T. (2022). *The EGS Collab – Initial Results from Experiment 2: Shear Stimulation at 1.25 km depth.* Paper presented at the 47th Workshop on Geothermal Reservoir Engineering, Sanford University.

Kneafsey, T. (2022). *The EGS Collab Project - Stimulations at Two Depths*. Paper presented at the ARMA Geomechanics Symposium, Santa Fe, New Mexico.

Kneafsey, T., Blankenship, D., Burghardt, J., Johnson, T. C., Dobson, P. F., Schwering, P., . . . Robertson, M. (2023). *The EGS Collab – Discoveries and Lessons from an Underground Experiment Series.* Paper presented at the 48th Workshop on Geothermal Reservoir Engineering, Stanford, CA.

Min, K. B., Rutqvist, J., Tsang, C. F., & Jing, L. R. (2004). Stress-dependent permeability of fractured rock masses: a numerical study. *International Journal of Rock Mechanics and Mining Sciences, 41*(7), 1191-1210. doi:10.1016/j.ijrmms.2004.05.005

Pyrak-Nolte, L., DePaolo, D. J., Pietra, T. . (2015). *Controlling Subsurface Fractures and Fluid Flow: A Basic Research Agenda.* . Retrieved from

Schmitt, D. R. (2015). Geophysical Properties of the Near Surface Earth: Seismic Properties. In G. Schubert (Ed.), *Treatise on Geophysics* (2 ed., Vol. 11, pp. 43-87): Elsevier.

Zoback, M. D., & Byerlee, J. D. (1975a). Effect of Microcrack Dilatancy on Permeability of Westerly Granite. *Journal of Geophysical Research, 80*(5), 752-755. doi:DOI 10.1029/JB080i005p00752

Zoback, M. D., & Byerlee, J. D. (1975b). Permeability and Effective Stress. *Aapg Bulletin-American Association of Petroleum Geologists, 59*(1), 154-158.